Design of a Low Micro Vibration High Precision CubeSat Reaction Wheel

Cedric Cuypers [(1)], Tjorven Delabie [(1)], Jelle Lanting [(1,2)], Wim De Munter[(2)], Rhimas Van de Putte [(1)], Joren Malfroy [(2)], Lubna Hamid [(1)]

[(1)] arcsec, Blijde Inkomststraat 22 Leuven Belgium, +32 498 817370, cedric@arcsecspace.com, tjorven@arcsecspace.com, jelle@arcsecspace.com, rhimas@arcsecspace.com, lubna@arcsecspace.com

[(2)] KU Leuven, Celestijnenlaan 300 Leuven Belgium, +32 16 32 24 80, jelle.lanting@kuleuven.be, wim.demunter@kuleuven.be, joren.malfroy@kuleuven.be

ABSTRACT

Missions involving payloads such as laser communications or astronomical objectives often have high pointing requirements. Arcsec is developing a CubeSat reaction wheel, dubbed "Zyra", in cooperation with the KU Leuven University and ESA under the GSTP program, to serve such demanding missions. The reaction wheel is a 160g wheel of 40x40x23mm^3 with a momentum capacity of 27.5mNm. The wheel has its own integrated power electronics which are tuned to the motor's low inductance and allowing full four quadrant control. It houses its own microprocessor and integrated control algorithms, allowing the reaction wheel assembly to function as a standalone unit with just a torque demand input from the ADCS controller. The ultimate goal of the project is to make a high-precision, low micro-vibration reaction wheel. To achieve this goal, the design of the wheels are balanced to ISO grade G0.4 and a preloaded suspension system is used while keeping the housing rigid and stiff to avoid resonances at low frequencies. To further improve the micro-vibration performance, the rotor structure is damped using constrained layer damping. Such a system allows to damp the rotor resonance frequencies while keeping the advantages of a single piece rotor and leaving the stiffness, mass and dimensions virtually unaffected.

1 INTRODUCTION

Missions involving payloads such as laser communications or astronomical objectives often have high pointing requirements. The lower budgets and small inertias of CubeSats and SmallSats increase the difficulty of achieving these pointing requirements for payloads mounted on such satellites. Reaction wheels are almost always employed as the actuators of choice for the fine pointing of satellites to achieve high precision pointing. Contradictory, they also belong to the instruments which limit the pointing accuracy that can be attained by the spacecraft, as they often represent one of the main sources of vibrations to the platform. This results in a delicate trade-off during the reaction wheel design. For example, reducing the dimensions and mass of a reaction wheel while maintaining a similar momentum capacity can be obtained by increasing the operating speed of the wheel, but comes at the cost of increased exported vibrations and power consumption.

Arcsec has been working on such a CubeSat reaction wheel, dubbed "Zyra" and shown in Figure 1, in cooperation with the KU Leuven and ESA under the GSTP program. The product of this design

effort is a 40x40x23mm^3 reaction wheel of 160g, providing 27.5mNm momentum capacity. The project is now entering its qualification and testing phase. A number of strategies were integrated into the design to increase the precision of the wheel.

Figure 1: Zyra reaction wheel

2 CONTROL & ELECTRONICS

Zyra has its own drive electronics, the required sensors, and a microcontroller integrated in its housing. This allows the wheel to function as a stand-alone device with custom control algorithms tuned to the reaction wheel behaviour. The drive electronics are custom designed and tuned to the low inductance motor and allow full four-quadrant control in a wide velocity range, as well as a braking resistor to ditch excess energy generated during deceleration of the wheel.

The control loop continuously estimates the friction encountered in the bearings during operation. The estimated friction is then added to the torque demand from the ADCS, which allows the wheel to quickly respond to friction changes and restore the angular velocity in such an event. The ADCS controller itself does not need to take into account such effects, or motor dynamics, and simply passes a torque demand to the integrated reaction wheel controller. Such a control architecture ultimately results in lower torque fluctuations, lower response times to unpredictable friction changes, and more stable control of the reaction wheel velocity.

3 MECHANICS

The mechanical construction of Zyra allows to reduce the effect of the most common vibration sources. The rotor is balanced in a field-balancing set-up to reduce the unbalance in its assembled configuration, and the bearing suspension is preloaded to avoid rattling and increase bearing life. To reduce the amplification of bearing harmonics, some damping mechanism is implemented in the rotor construction to further improve the micro-vibration behavior.

3.1 Balance & Preload

In a first effort to reduce exported vibrations, Zyra's rotor is balanced down to grade G0.4. Rotor unbalance shows up in the exported vibration spectrum on the rotational frequency of the flywheel. Rotor balancing can in general be performed in 2 ways. In rotor balancing, the rotor is balanced prior to assembly. In field balancing, the rotor is first integrated in the system and balanced afterwards. This second method allows to take some effects of the assembly into account. When working with small bearings, there are a number of challenges to this approach. During balancing, material is either removed or added to the rotor. To add material, threaded holes are required in the circumference of the rotor, increasing the rotor complexity, production cost and potentially lowering the nominal mass of the flywheel. Removing material can be challenging without damaging the bearings, and preventing them from contamination with dust. Taking the envisioned balancing method into account during the assembly design allows to use less conventional balancing methods. Zyra's housing is therefore designed to allow laser ablation post-assembly during the balancing procedure. In this process, performed by an external partner, a laser is used to remove material from the rotor while simultaneously measuring the remaining unbalance on the rotor. This allows to balance the reaction wheel in a field-balancing set-up to ISO grade G0.4 without damaging or contaminating the bearings. A last assembly step allows to close off the rotor completely and protect it against contamination or scratches which might compromise the balancing grade.

To avoid rattling in the bearings, as well as to increase the bearing lifetime, the bearings of Zyra are axially preloaded. When no preload is applied to the system, production tolerances and thermal fluctuations might cause either excessive clearance in the bearings or cause the elements to become squeezed to hard. The preload is applied to the bearings through a spring in a so called soft-preload suspension. It utilizes a preload screw to repeatably set the desired preload to the bearings independent of production tolerances, as well as a loaded spring to keep the actual preload within the desired limits over the entire operating temperature range. By using a dedicated spring and a sliding fit on one of the bearing interfaces, the housing can be kept rigid and stiff to avoid resonances at low frequencies.

3.2 Rotor Construction

Another source of vibrations are amplification of higher order harmonics by the rotor modes, which can become higher in amplitude than the unbalance for carefully balanced systems. Rolling element bearings are known to generate higher order harmonics. Even 10^{th} or higher engine orders can be observed, depending on the bearing type [1]. An example of such harmonics is shown in Figure 2. When rotors are used in a wide speed range, such high order harmonics might pass and excite the rotor modes, resulting in large amplifications and an increase in exported micro vibrations.

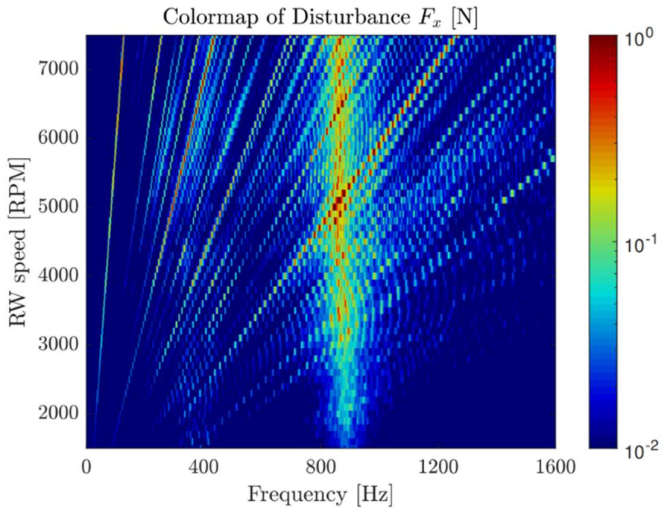

Figure 2: Colormap of disturbance forces on a rotating system

This amplification depends on the quality factor (Q-factor) of the rotor structure. The Q-factor is a measure for how underdamped a certain structure is, and is defined as in equation (1).

$$Q = \frac{f_c}{\Delta f_{-3dB}} \tag{1}$$

With f_c the resonance frequency of the mode and Δf_{-3dB} the width of the peak where the application has dropped with 3dB with respect to the tip of the peak.

Monolithic metallic structures, in general, have high Q-factors. This means the response of the structure is highly underdamped and the amplification of vibrations at these frequencies will be large.

Still, there are some advantages to single piece rotors. Having the whole structure, including the shaft, web and rim machined as a single structure allows for tighter tolerances and uniform mass distribution as they can be machined in one or two machine clampings, and do not suffer misalignment due to assembly or changes in alignment due to thermal stresses.

However, as they lack friction in e.g. joints and fasteners, the only damping of resonance frequencies comes from the internal damping of the material itself, which is low for metals. Still there are some differences in this internal damping exhibited by different alloys, and it can be an important parameter during the material selection of the rotor. For this reason, Zyra's rotor is manufactured from bronze. Bronze has higher internal damping compared to steel [1], which in combination with its high density and corrosion and fatigue resistance is a favourable characteristics for a single piece rotor.

But material selection is not the only attempt at decreasing the Q-factor. This problem of low damping of monolithic metallic structures is found in other areas as well. In some cases a Constrained Layer Damping (CLD) construction is employed to significantly increase the damping while leaving other characteristics of the structure such as size, stiffness, mass and resonance frequencies largely unaffected [2].

The principle of CLD is to add a viscoelastic material to the structure in such a way that the viscoelastic material is deformed in shear deformation when the base structure is bent, see Figure 3. This way, the viscoelastic material shows large deformations relative to the base structure under vibrational loads. When a simple damping layer of such a material is added to a base structure surface, the damping layer is deformed in tension or compression upon deformation of the base structure. In doing so, energy is dissipated due to the viscous nature of the material. The amount of energy dissipated is dependent on the deformation in the viscoelastic layer and is for this configuration dependent on the tension/compression strain in the layer [3]. Displacement in the damping layer is in such case of the same order of magnitude compared to the displacement of the base itself, which are limited when stiff structures are desired.

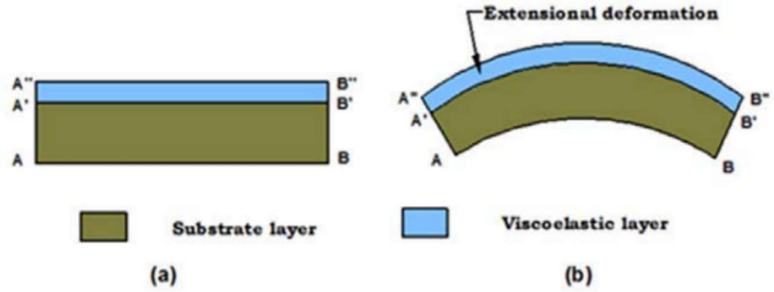

Figure 3: Unconstrained layer damping [3]

When an additional layer is added to the top of the viscoelastic layer the top of the layer becomes "constrained", as shown in Figure 4. This forces the entire viscoelastic interlayer to deform in shear deformation for a similar base structure deformation. This deformation in shear strain has much larger relative deformation compared to tension or compression, resulting in more efficient energy dissipation for a similar base structure deformation, even if a thin viscoelastic interlayer is added [3].

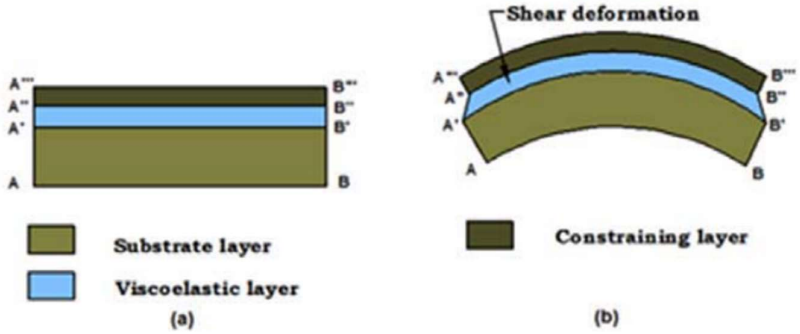

Figure 4: Constraint layer damping [3]

To further increase the damping of the rotor, this principle was added to the web of the rotor. Three different stack-ups were manufactured and tested on a shaker set-up for comparison with a baseline rotor without any viscoelastic interlayer. Although the actual rotor is made from bronze, the 4 test rotors were manufactured from steel. This was done to amplify the effect of the damping layer, as well as to save cost. The rotor yoke and magnets are replaced with a representative dummy ring of approximately equal mass and dimensions.

For the calculation of the dimensions of the interlayer and constraining layer, the analytical formulations for CLD on plate structures applied to the cross section of the flywheel web was used as starting point. As the web of the outrunner is conical rather than flat, using plate bending is a very

rough estimation, as the complex bending stiffnesses for plates and cone surfaces differ. However, the driving principles which affect the efficiency of the damping in the structure are similar and can be used for a relative estimation between the efficiency of different CLD constructions of the flywheel.

The parameters and formulas used, adopted from [2] and [4], are shown in equations (2) to (7).

$$X = \frac{G_2}{p^2 h_2} S \tag{2}$$

$$S = \frac{1}{E_1 h_1} + \frac{1}{E_3 h_3} \tag{3}$$

$$\frac{1}{p^2} = \frac{1}{\omega} \sqrt{\frac{\vec{B}}{\mu}} \tag{4}$$

$$\vec{B} = \frac{1}{12} (E_1 h_1^3 + E_3 h_1^3) \left(1 + \frac{X^* Y}{1 + X^*}\right) \tag{5}$$

$$X^* = X(1 - j\beta) \tag{6}$$

$$X_{opt} = [(1 + Y)(1 + \beta^2)]^{-1/2} \tag{7}$$

With:

Symbol	Explanation
X	Shear parameter
$\vec{B}$	Complex bending stiffness
Y	Structural parameter
β	Loss factor of the viscoelastic material
μ	Mass per area of the composite structure
ω	Angular frequency of interest to optimize for

In the first rotor, the viscoelastic interlayer is added in the centre of the web. The web is split in half making the base layer and constraining layer approximately equally thick. The constraining layer is pressed into the rotor underneath the yoke dummy with a press fit on its outer circumference and a loss transition fit around the shaft. This results in a fit where the interlayer is fully closed off and the constraining layer is supported around its entire circumference.

In the second rotor, the constraining layer is added from the top side. More of the web is retained and the interlayer is no longer located on the neutral axis of the bending mode. The constraining layer is open at the outer circumference and a loose transition fit around the shaft.

The third stack-up is similar to the second, but with greatly reduced interlayer and constraining layer thickness. The three rotor constructions are shown in Figure 5.

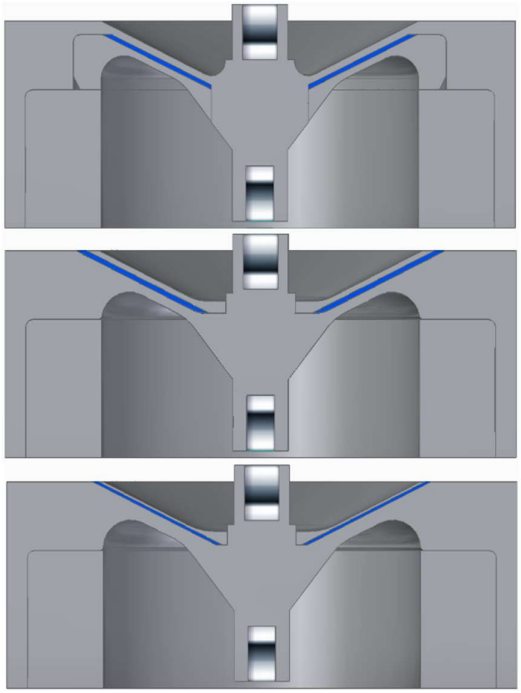

DR1
Base: 0,47mm
Interlayer: 0,31mm
Constraining layer: 0,5mm
Constraining layer pressed and fully closed

DR2
Base: 0,71mm
Interlayer: 0,35mm
Constraining layer: 0,4mm
Constraining layer loose and open at sides

DR3
Base: 0,98mm
Interlayer: 0,2mm
Constraining layer: 0,15mm
Constraining layer loose and open at sides

Figure 5: Damped rotor stack-ups

These 4 rotors were mounted on a shaker set-up and a resonance search was performed between 5 and 2500Hz. This upper limit was selected as the highest mode which can be excited by a 10th engine order harmonic at the maximal rotational rate intended for the rotor. An overlay of all 4 rotors' responses is shown in Figure 6.

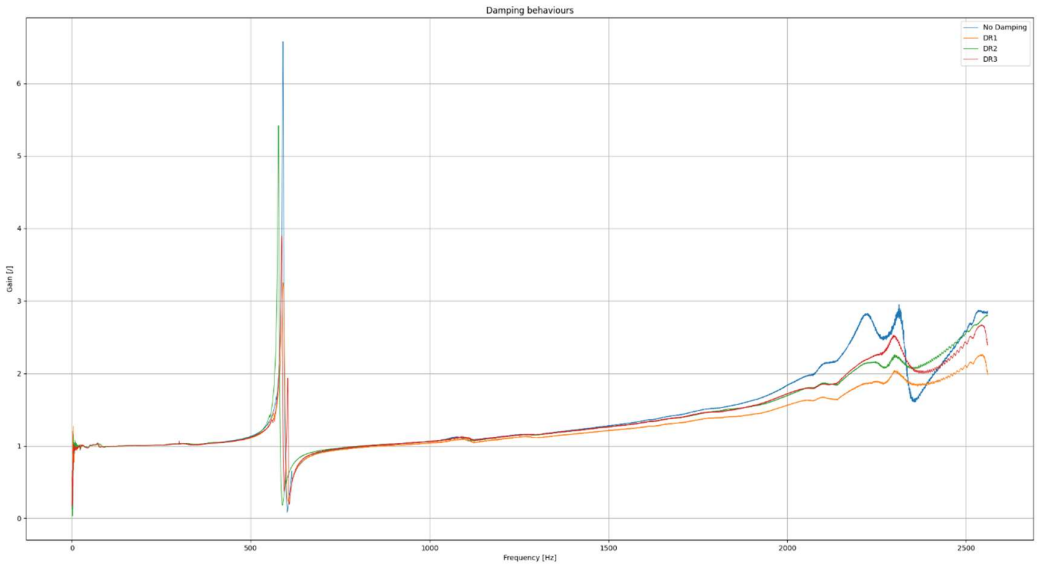

Figure 6: Damped rotos responses

At higher frequencies, all of the damped rotors show improved behaviour, although rotor 1 shows the highest reduction in response. In the mid frequency range, all 4 plots fall together around an amplification of 1, slowly deviating as the frequency increases. The damping layer having little effect in this range is to be expected. An amplification of 1 on the acceleration response spectrum indicates

inertial behaviour, as if the system resembles a solid body. With no tensional or shear deformation in the damping material, the interlayer will have little effect on the dynamic characteristics of the system.

The most interesting region is the range around the first resonance frequency of the rotors, shown in Figure 7.

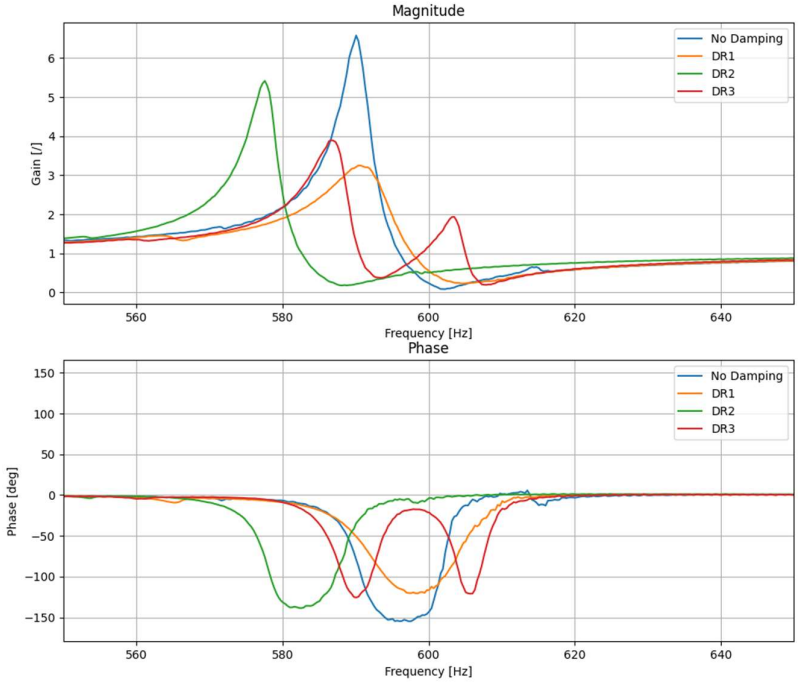

Figure 7: First rotor resonance

Rotor 2 and 3 behave as a tuned mass damper. The initial resonance peak is for both these rotor constructions split into 2 smaller peaks, left and right of the original peak in the frequency domain. For rotor 3 this is clearly visible. For rotor 2, the second peak is quite small, and mainly visible in the phase diagram only. Both of these rotors have a similar construction, with only variations in thicknesses of the layers, but not the way they are employed. For both these rotors, the constraining layer has 1 open side and 1 loose fit on the shaft. As such, the constraining layer is only supported through the constraining layer and not directly fixed to the base structure, such as for rotor 1. As this can be seen as a flexible connection, the tuned mass damper like behaviour can be explained.

For rotor 2, the damping exhibited in the peaks is limited compared to the undamped rotor. Rotor 3 has somewhat higher damped peaks, but still not the comparable to the expected potential of CLD [2]. This suggests that for this CLD topology the inter layer does not sufficiently go into shear deformation. Rather, the obtained effect is that of a tuned pass damper [6]. Although the resonances are reduced in amplitude, the amplification is now present in 2 frequency bands, which can be undesirable in the application of a low micro-vibration reaction wheel.

For rotor 1, the effect of the damping interlayer is better visible. No additional resonance frequencies are found, but the peak shows increased damping behavior. To quantify the increase in damping with respect to the undamped rotor, the Q-factors of both systems are compared.

The Q-factors are calculated as per equation (1). This is visually represented in Figure 8.

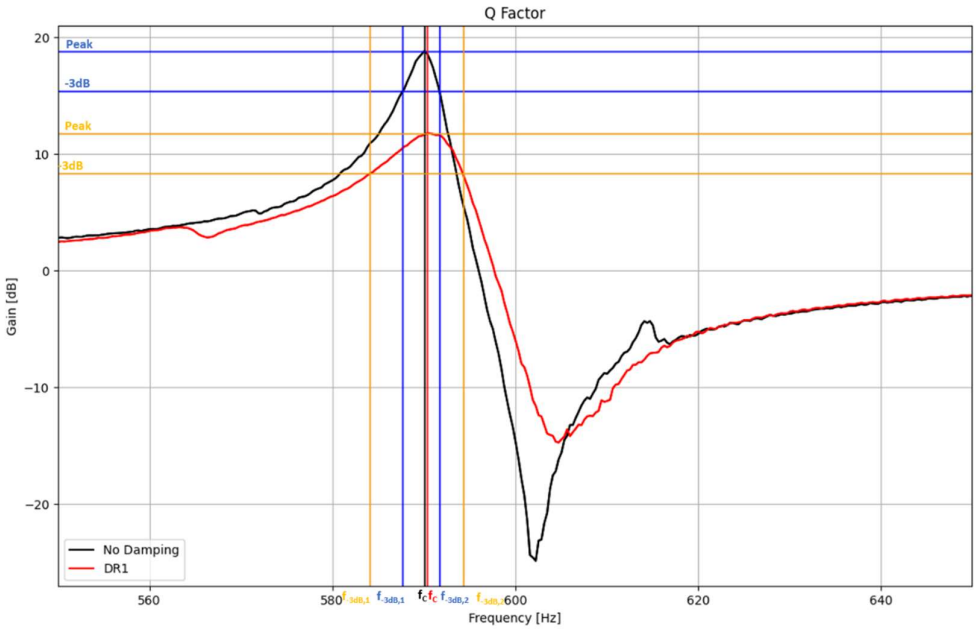

Figure 8: Q-factor representation

The resulting Q-factors and damping coefficients are listed in Table 1 together with their respective resonance frequency, with damping coefficient as is equation (8).

$$\frac{1}{Q} = 2\zeta \tag{8}$$

Table 1: Damped vs undamped rotor comparison

Rotor	Q-factor [/]	Damping coefficient [/]	Resonance frequency [HZ]
Undamped	146.04	0.0034	590.07
DR1	58.09	0.0086	590.39

This equates to a 59.2% drop in Q-factor for the damped rotor, with the addition of a 0.3mm thick viscoelastic interlayer.

When comparing the resonance location, no significant shift in frequency is observed between the 2 systems. Given that the rotors are otherwise similar in mass and dimensions, it is concluded that the stiffness of the rotor remained generally unaffected by the addition of the interlayer. This behavior of increased damping with little effect on the other parameters, is the targeted effect of the CLD strategy that was here employed. This rotor lay-out was therefore selected and implemented in Zyra's rotor construction, albeit with a bronze base and constraining layer in favor of steel.

4 FUTURE PROSPECTS

The next phase in the project is the validation of the implemented mechanisms and the environmental test campaign. The initial vibration tests performed on the separate rotors show the effect of the CLD on the rotor structure. This alone does not guarantee an improved micro-vibration spectrum at system level. As the rotor structure is supported by the bearings, the damping present in the bearings themselves might overshadow the effect of the increased rotor damping. To validate the effect of the CLD implementation into the rotor on the micro-vibration spectrum, a more high-level test is required. One reaction wheel assembly with a solid, undamped rotor will be compared for micro-vibration measurements with an assembly with the CLD rotor.

In the coming months, the wheel will go consecutively through vibration, shock and TVAC tests, as well as accelerated lifetime tests for a design lifetime of 5 years in orbit and TID and SEE radiation tests on the PCBs and most sensitive ICs. At the end of the environmental test campaign, the wheels will again be tested on exported micro-vibration to validate their performance and robustness.

5 REFERENCES

[1] S. J. Lacey, *An Overview of Bearing Vibration Analysis,* Schaeffler Group.

[2] J. Zhang, R. J. Perez and E. J. Lavernia, "Documentation of damping capacity of metallic, ceramic and metal-matrix composite materials," *JOURNAL OF MATERIALS SCIENCE,* vol. 28, pp. 2395-2404, 1993.

[3] J. de Vreugd, D. de Lange, J. Winters, J. Human, F. Kamphues and E. Tabak, "DAMPING IN SPACE CONSTRUCTIONS," in *13th European Conf. on Spacecraft Structures, Materials & Environmental Testing*, Braunschweig, 2014.

[4] A. Kumar and R. K. Behera, "Passive Constrained Layer Damping: A state of the Art Review," in *International Conference on Advances in Materials and Manufacturing Engineering* , Bhubaneswar, 2019.

[5] B. M. Shafer, "An overview of constrained-layer damping theory and application," in *Structural Acoustics and Vibration*, Montreal, 2013.

[6] M. Gaspar, "The mechanism and applications of a Tuned Mss Damper (TMD)," BSB Group, 22 11 2017. [Online]. Available: https://bsbgroup.com/blog/the-mechanism-and-applications-of-tuned-mass-damper-tmd#:~:text=What%20is%20a%20Tuned%20Mass,earthquake%20or%20high%20winds%20hit.. [Accessed 23 11 2022].